Analysis of Microstrip Resonators of Arbitrary Shape

Krzysztof A. Michalski, *Senior Member, IEEE,* and Dalian Zheng, *Member, IEEE*

Abstract—**A space-domain approach based on a mixed-potential integral equation formulation is developed for efficient computation of complex resonant frequencies of laterally open microstrip-patch resonators of arbitrary shape. The effects of the substrate—which may consist of any number of planar, possibly uniaxially anisotropic, dielectric layers—are rigorously incorporated in the formulation by means of the vector and scalar potential Green's functions. The current distribution on the conducting patch is approximated in terms of vector basis functions defined over triangular elements. Computed resonant frequencies, quality factors, modal currents, and far-field radiation patterns are presented for several microstrip resonators. For patches of simple, regular shapes, the results are in agreement with published data obtained by specialized techniques, which—unlike the method presented here—are not easily extendable to arbitrary shapes.**

I. Introduction

IN THE microwave frequency band, microstrip-patch resonators of various shapes are used as antennas and as components in integrated-circuit oscillators and filters. These resonators have narrow bandwidths and can only operate effectively in the vicinity of the resonance frequency. Therefore, it is important in these applications to accurately ascertain the resonance frequencies of the resonators. Previous rigorous analyses of microstrip resonators have relied on the spectral domain integral equation approach [1]–[5]. This technique, which depends on the availability of Fourier-transformable expansion functions, has traditionally been limited to microstrip patches of a few simple shapes. Recently, the present authors [6] have demonstrated that this approach is feasible for the analysis of planar, but otherwise arbitrarily shaped microstrip structures, modeled by triangular elements. It has been concluded, however, that—unless a breakthrough is achieved in the acceleration of the slowly convergent double spectral integrals that arise—the spectral domain approach is not competitive in terms of efficiency with the state-of-the-art space domain methods, especially those based on the mixed-potential integral equation (MPIE) [7], [8]. The MPIE approach has first been used in the analysis of microstrip structures by Mosig and Gardiol [9], who applied it in conjunction with the "rooftop" basis functions [10] defined over rectangular subdomains. Although the rectangular-mesh model has successfully been used to analyze planar microstrip structures of various shapes [11]–[13], a triangular-element model is applicable to a still wider class of geometries. This has recently been recognized by several authors [14]–[16], who employed the MPIE formulation in conjunction with the vector basis functions defined over a triangular support [17]. In this paper, we adopt the latter approach to study laterally open microstrip resonators of planar, but otherwise arbitrary shape, embedded in a layered, possibly uniaxial medium.

Manuscript received March 27, 1991; revised July 9, 1991. This work was supported in part by the Office of Naval Research under Contract N00014-90-J-1197.

The authors are with the Electromagnetics and Microwave Laboratory, Department of Electrical Engineering, Texas A&M University, College Station, TX 77843-3128.

IEEE Log Number 9103896.

II. Formulation

We consider the structure of Fig. 1, where the time variation of the electromagnetic field is assumed to be specified by an $e^{j\omega t}$ factor, which is suppressed throughout. Here, $\omega = 2\pi f$, where f is the (in general complex) frequency. The free-space permeability and permittivity are denoted by μ_0 and ϵ_0, respectively, and the free-space wavenumber and characteristic impedance are given by $k_0 = \omega\sqrt{\mu_0\epsilon_0}$ and $\eta_0 = \sqrt{\mu_0/\epsilon_0}$, respectively. The dielectric medium in Fig. 1 is uniform and of infinite extent along the x and y coordinates, and so is the ground plane. The dielectric layers may be uniaxially anisotropic with the optic axis parallel to the z axis [18, p. 745]. The nth layer is characterized by the permittivity tensor $\underline{\underline{\epsilon}}_n = [\underline{\underline{I}} + \hat{z}\hat{z}(\nu_n - 1)]\epsilon_{tn}$, where $\underline{\underline{I}}$ is the idemfactor, $\nu_n = \epsilon_{zn}/\epsilon_{tn}$ is the anisotropy ratio, and ϵ_{tn} and ϵ_{zn} denote, respectively, the transverse and longitudinal dielectric constants of the nth layer, relative to free space. Here and throughout this paper, unit vectors are distinguished by carets and dyadics by double underlines. The patch resonator is assumed to be planar, with negligible thickness, but its shape may be arbitrary and is modeled by triangular finite elements, as indicated in Fig. 1. The patch and the ground plane are assumed to be made of a perfect electric conductor (PEC). If desired, the effects of finite conductivity may be incorporated by means of the surface impedance concept [11]. Although the formulation presented here is applicable to multi-layer and multi-patch structures, in this paper we focus attention on the case of a single patch on a grounded substrate of thickness h with, possibly, a superstrate of thickness d.

The problem of Fig. 1 may be replaced by its equivalent [19, p. 106], in which the conducting patch S has been removed and its effect replaced by an electric surface current with density J_S. The magnetic and electric fields,

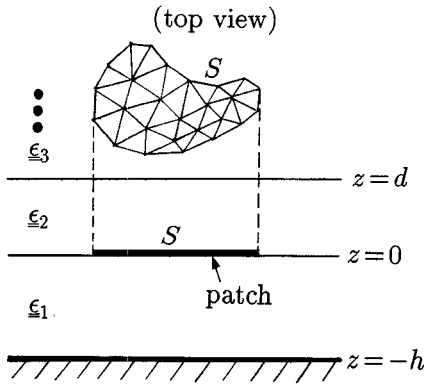

Fig. 1. Geometry of an arbitrarily shaped microstrip patch resonator.

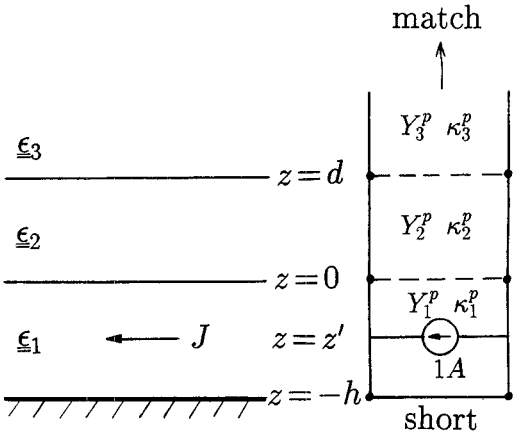

Fig. 2. Layered dielectric medium and its transmission-line network analogue.

$\boldsymbol{H}$ and $\boldsymbol{E}$, respectively, due to $\boldsymbol{J}_S$, can be expressed as

$$\mu_0 \boldsymbol{H}(\boldsymbol{r}) = \nabla \times \boldsymbol{A}(\boldsymbol{r}) \tag{1}$$

$$-\boldsymbol{E}(\boldsymbol{r}) = j\omega \boldsymbol{A}(\boldsymbol{r}) + \nabla \Phi(\boldsymbol{r}) \tag{2}$$

where $\boldsymbol{A}$ and Φ denote, respectively, the vector and scalar potentials, and $\boldsymbol{r}$ is the position vector. The vector potential is given as

$$\boldsymbol{A}(\boldsymbol{r}) = \int_S \underline{\underline{G}}^A(\boldsymbol{r}|\boldsymbol{r}') \cdot \boldsymbol{J}_S(\boldsymbol{\rho}')\, dS' \tag{3}$$

with the dyadic kernel

$$\underline{\underline{G}}^A(\boldsymbol{r}|\boldsymbol{r}') = (\hat{x}\hat{x} + \hat{y}\hat{y}) G_{xx}^A(\boldsymbol{r}|\boldsymbol{r}') + \hat{z}\hat{x} G_{xx}^A(\boldsymbol{r}|\boldsymbol{r}') + \hat{z}\hat{y} G_{zy}^A(\boldsymbol{r}|\boldsymbol{r}'). \tag{4}$$

Here and throughout, primes indicate source coordinates, $\boldsymbol{\rho}$ is the projection of $\boldsymbol{r}$ on the xy-plane, and the subscript S distinguishes vectors that are transverse to $\hat{z}$. The scalar potential in (2) is given as

$$\Phi(\boldsymbol{r}) = -\frac{1}{j\omega} \int_S G^\phi(\boldsymbol{r}|\boldsymbol{r}') \nabla_S' \cdot \boldsymbol{J}_S(\boldsymbol{\rho}')\, dS' \tag{5}$$

where the kernel G^ϕ may be interpreted as the scalar potential of a single point charge associated with a horizontal Hertzian dipole [9], [20]. Using the notation

$$\mathcal{S}_n\{f(k_\rho)\} = \frac{1}{2\pi} \int_0^\infty f(k_\rho) J_n(k_\rho \xi) k_\rho^{n+1}\, dk_\rho, \tag{6}$$

$$n = 0, 1, 2$$

$$\xi = \sqrt{(x-x')^2 + (y-y')^2}, \tag{7}$$

$$\zeta = \tan^{-1}\left(\frac{y-y'}{x-x'}\right)$$

where J_n is the Bessel function of order n, the elements of the dyadic (4) can be expressed as [21]

$$j\omega G_{xx}^A(\boldsymbol{r}|\boldsymbol{r}') = \mathcal{S}_0\{V_i^h(z|z')\} \tag{8}$$

$$j\omega G_{zx}^A(\boldsymbol{r}|\boldsymbol{r}') = -jk_0\eta_0 \cos\zeta \mathcal{S}_1\left\{\frac{I_i^h(z|z')}{k_\rho^2} - \frac{I_i^e(z|z')}{k_\rho^2}\right\} \tag{9}$$

with G_{zy}^A given by (9) with cos ζ replaced by sin ζ. The scalar potential kernel G^ϕ in (5) is given as

$$-\frac{1}{j\omega} G^\phi(\boldsymbol{r}|\boldsymbol{r}') = \mathcal{S}_0\left\{\frac{V_i^h(z|z')}{k_\rho^2} - \frac{V_i^e(z|z')}{k_\rho^2}\right\}. \tag{10}$$

As an aid in deriving these expressions, we have employed the transmission-line network analogue of the layered medium [18, Ch. 2], as illustrated in Fig. 2. This network actually represents two networks (having identical configurations, but in general different propagation constants and characteristic impedances) that arise from the decomposition of the electromagnetic field into partial fields that are transverse-magnetic (TM) and transverse-electric (TE) to $\hat{z}$ [22]–[26]. The quantities associated with the TM and TE networks are distinguished by the superscripts e and h, respectively. The kernel functions in (8)–(10) are expressed in terms of the voltage and current transmission-line Green's functions, V_i^p and I_i^p, where p stands for e or h [25]. For easy reference, the transmission-line Green's functions pertinent to the three-layer configuration of Fig. 1 are listed in the Appendix.

In the absence of external excitation, the tangential component of the electric field given by (2) must vanish on the PEC surface S, which leads to the MPIE

$$j\omega \int_S G_{xx}^A(\boldsymbol{r}|\boldsymbol{r}') \boldsymbol{J}_S(\boldsymbol{r}')\, dS' - \frac{\nabla_S}{j\omega} \int_S G^\phi(\boldsymbol{r}|\boldsymbol{r}') \nabla_S' \cdot \boldsymbol{J}_S(\boldsymbol{\rho}')\, dS' = 0, \qquad \boldsymbol{r} \in S. \tag{11}$$

This homogeneous equation has nontrivial solutions at the resonance frequencies of the structure, which are complex, thus reflecting the loss of energy due to radiation. A resonance frequency f may be expressed as

$$f = f_r\left(1 + \frac{j}{2Q}\right) \tag{12}$$

Here, f_r is the real part of f and Q is the quality factor (Q-factor, for short), where usually $Q >> 1$. Once a resonance frequency and the corresponding modal current distribution $\boldsymbol{J}_S$ is determined, other quantities of interest, such as the far-zone field, can be found with little extra

effort. The latter may be easily computed from (2) if we note that far from a localized source the contribution due to the scalar potential may be neglected [19, p. 133]. If we assume that the observation point is above the upper interface (i.e., $z > d$), the vector potential term in (2) can be easily evaluated by the stationary-phase method [27]. As a result, the far field components of the electric field in the upper half-space—which is assumed here to be characterized by free space parameters—are found as

$$E_{\theta,\varphi}(\boldsymbol{r}) \sim \frac{e^{-jk_0 r}}{jk_0 r}\, \mathcal{E}_{\theta,\varphi}(\hat{\boldsymbol{r}}) \tag{13}$$

where r, θ, and φ are the usual spherical coordinates, and where $\mathcal{E}_\theta$ and $\mathcal{E}_\varphi$ are the far field pattern functions, given as

$$\mathcal{E}_{\theta,\varphi}(\hat{\boldsymbol{r}}) = \frac{k_0^2}{2\pi}\, e^{jk_0 d\cos\theta}\, \boldsymbol{G}_{\theta,\varphi}(\hat{\boldsymbol{r}}|z') \cdot \int_S \boldsymbol{J}_S(\boldsymbol{\rho}')\, e^{jk_0\hat{\boldsymbol{r}}\cdot\boldsymbol{\rho}'}\, dS' \tag{14}$$

with

$$\hat{\boldsymbol{r}}\cdot\boldsymbol{\rho}' = (x'\cos\varphi + y'\sin\varphi)\sin\theta.$$

Here, we have introduced

$$\boldsymbol{G}_\theta(\hat{\boldsymbol{r}}|z') = V_i^e(d|z')\,\hat{\boldsymbol{\rho}}, \quad \boldsymbol{G}_\varphi(\hat{\boldsymbol{r}}|z') = \cos\theta V_i^h(d|z')\,\hat{\boldsymbol{\varphi}} \tag{15}$$

where the voltage Green's functions are evaluated at the stationary-phase point value of $k_\rho = k_0 \sin\theta$. If the cover layer is absent, we simply put in the above $d = 0$. We note from (13) that, since $\Im mk_0 > 0$, the far-field natural mode grows without bound as $r \to \infty$. It can be shown, however, that when the time dependence is restored and the requirements of causality are satisfied, this mode exhibits the expected damped, oscillatory time behavior [28].

It should be noted that the equivalent current $\boldsymbol{J}_S$ represents a vector sum of the currents $\boldsymbol{J}_{S+}$ and $\boldsymbol{J}_{S-}$ that exist, respectively, on the top and bottom sides of the patch S in the original problem [29]. Once $\boldsymbol{J}_S$ and the resulting magnetic field have been found, the currents on both sides of the patch can be determined as

$$\boldsymbol{J}_{S\pm}(\boldsymbol{\rho}) = \pm\hat{\boldsymbol{z}} \times \boldsymbol{H}(\boldsymbol{r}), \qquad \boldsymbol{r} \in S_\pm \tag{16}$$

where $\boldsymbol{r}$ approaches S from above or from below at a location specified by $\boldsymbol{\rho}$.

III. Numerical Method

As indicated in Fig. 1, we model the microstrip patch by triangular elements. To solve the MPIE (11), we adopt the moment method [30] in conjunction with the vector basis functions defined over triangular subdomains [17]. Below, we summarize this approach using an efficient notation similar to that commonly used in the finite elements literature [31].

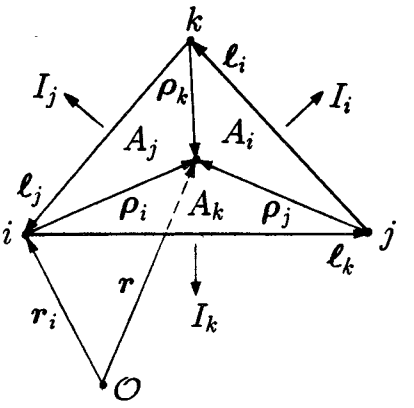

Fig. 3. Local coordinates associated with a triangular element. The element number superscripts have been omitted.

A. Patch Current Expansion

The nodes of each triangular element are assigned the indices i, j, and k in the counterclockwise direction, as illustrated in Fig. 3. Here, we adopt a local indexing scheme, in which these indices assume the values 1, 2, or 3 in a cyclic manner. The sides of the nth triangle S_n with an area $A^{(n)}$ are formed by three edge vectors $\boldsymbol{l}_i^{(n)}$, $i = 1, 2, 3$, with $\boldsymbol{l}_i^{(n)}$ oriented from node j to node k. The ith node of S_n is defined with respect to the global coordinate origin $\mathcal{O}$ by a position vector $\boldsymbol{r}_i^{(n)}$. The patch current distribution on S_n is approximated as

$$\boldsymbol{J}_S^{(n)}(\boldsymbol{\rho}) = \sum_{i=1}^{3} I_i^{(n)} \boldsymbol{\Lambda}_i^{(n)}(\boldsymbol{\rho}) \tag{17}$$

where $I_i^{(n)}$ is the total current leaving the ith edge, and $\boldsymbol{\Lambda}_i^{(n)}$ is a vector basis function defined as [17], [32], [33, p. 449], [34], [35]

$$\boldsymbol{\Lambda}_i^{(n)}(\boldsymbol{\rho}) = \frac{\boldsymbol{\rho}_i^{(n)}}{2A^{(n)}}, \quad \boldsymbol{\rho}_i^{(n)} = \boldsymbol{l}_k^{(n)} L_j - \boldsymbol{l}_j^{(n)} L_k. \tag{18}$$

Here, L_i is the area coordinate associated with the ith node [31, p. 110], and is given as

$$L_i = \frac{A_i^{(n)}}{A^{(n)}}, \quad \sum_{i=1}^{3} L_i = 1 \tag{19}$$

where $A_i^{(n)}$ is the area of the triangle formed by the observation point within the nth element and its nodes with indices j and k (see Fig. 3). The position vector of an arbitrary point on S_n may be expressed in terms of the area coordinates as

$$\boldsymbol{r} = \boldsymbol{r}_i^{(n)} + \boldsymbol{\rho}_i^{(n)}, \qquad i = 1, 2, 3. \tag{20}$$

The divergence of $\boldsymbol{J}_S^{(n)}$ is readily found as

$$\nabla\cdot\boldsymbol{J}_S^{(n)}(\boldsymbol{\rho}) = \sum_{i=1}^{3} \frac{I_i^{(n)}}{A^{(n)}} \tag{21}$$

Hence, in view of the equation of continuity, the charge density associated with the current (17) is constant over an element. When the expansions (17) and (21) are substituted into the integral equation (11), the coefficients

$I_i^{(n)}$ are constrained by the boundary conditions, which require the continuity of the normal components of $\boldsymbol{J}_S$ across the edges shared by adjacent elements, or their vanishing at the boundary edges of S.

B. Testing Procedure and Matrix Assembly

In the solution procedure, the current expansion functions described above are substituted into the "weak form" of the integral equation (11), which is obtained by "testing" it with the same basis functions as those used to represent the current. Hence, to obtain the weak form of (11) on, say, the mth triangular element, we take a dot product of both sides of this equation with $\boldsymbol{\Lambda}_l^{(m)}$ ($l = 1, 2, 3$) and integrate the result over S_m. Next, we apply a Gauss theorem [36, p. 503] to the gradient term and—to reduce the computational effort—use a one-point rule to approximate the testing integrals. As a result, we obtain

$$j\omega \int_S G_{xx}^A(\boldsymbol{r}_c^{(m)}|\boldsymbol{r}')\boldsymbol{\rho}_{cl}^{(m)} \cdot \boldsymbol{J}_S(\boldsymbol{\rho}')\, dS' - \frac{2}{j\omega}\int_S G^{\phi}(\boldsymbol{r}_c^{(m)}|\boldsymbol{r}')\nabla_S' \cdot \boldsymbol{J}_S(\boldsymbol{\rho}')\, dS' = 0 \quad (22)$$

where the center of gravity of S_m is specified by the global position vector $\boldsymbol{r}_c^{(m)}$, and also by the local vector $\boldsymbol{\rho}_{cl}^{(m)}$, where the latter originates at the lth node of the mth element. To determine the contribution of the current on the nth element, we substitute in the above the expansions (17) and (21), which leads to a system of linear equations

$$\sum_{i=1}^{3} z_{li}^{(mn)} I_i^{(n)} = 0, \qquad l = 1, 2, 3 \quad (23)$$

where the impedances $z_{li}^{(mn)}$ are given as

$$z_{li}^{(mn)} = j\omega\boldsymbol{\rho}_{cl}^{(m)} \cdot \boldsymbol{l}_k^{(n)} \int_0^1 \int_0^{1-L_j'} G_{xx}^A(\boldsymbol{r}_c^{(m)}|\boldsymbol{r}')L_j'\, dL_k'\, dL_j' - j\omega\boldsymbol{\rho}_{cl}^{(m)} \cdot \boldsymbol{l}_j^{(n)} \int_0^1 \int_0^{1-L_j'} G_{xx}^A(\boldsymbol{r}_c^{(m)}|\boldsymbol{r}')L_k'\, dL_k'\, dL_j' - \frac{4}{j\omega}\int_0^1 \int_0^{1-L_j'} G^{\phi}(\boldsymbol{r}_c^{(m)}|\boldsymbol{r}')\, dL_k'\, dL_j'. \quad (24)$$

Here, the integrals over S_n have been expressed in terms of the area coordinates [17]. Because the latter are related by (19), only three distinct integrals of G_{xx}^A and three distinct integrals of G^{ϕ} are involved in (24) as i ranges from 1 to 3. Moreover, each trio of integrals may be computed concurrently, so that one set of values of G_{xx}^A or G^{ϕ} is reused in three integrals. Hence, it may be said that only two distinct kernel integrals are required for each element pair (m, n). These two integrals, which contribute to nine impedance elements in (23), may be efficiently evaluated by a numerical quadrature especially developed for triangular domains [31, p. 113]. We use a seven-point rule when the source and test elements are close to each other, and four-point or one-point rules for widely separated element pairs. When $m = n$ in (24), the integrands are singular and must be handled with care. In this case, we extract from them the static singular terms and integrate them analytically using the formulas developed by Wilton *et al.* [37].

As there are no unknowns associated with the boundary edges of S, where the normal component of the surface current vanishes, we only need to find the normal currents I_q ($q = 1, \cdots, N$) associated with the N non-boundary edges in the triangular mesh approximation of S. There exists a unique mapping between the coefficients $I_i^{(n)}$ on each element and the edge currents I_q, whose reference directions are automatically specified by the order in which the node numbers appear in the mesh data. To determine I_q, we must first assemble the global $N \times N$ impedance matrix. The assembly process proceeds on the element-by-element basis. Hence, there are two nested loops in the computer program, with indices m and n, each ranging over all elements. For each pair of elements (m, n), we compute up to nine impedances $z_{li}^{(mn)}$, according to (24). Each of these impedances is then added—with the appropriate sign—to the element of the global impedance matrix corresponding to the pair of edge currents $(I_l^{(m)}, I_i^{(n)})$. We use the plus sign if the reference direction of the edge current is out of the element, and minus sign otherwise. After all element pairs are processed in this manner, (11) is converted into a homogeneous matrix equation, which has nontrivial solutions only at those frequencies, for which the matrix determinant vanishes. These resonance frequencies are found in the complex frequency plane by the Müller method [38, p. 120]. The determinant is computed using an LU factorization of the matrix as an intermediate step, and the non-boundary edge currents I_q are obtained by back-substitution, after one of them has been arbitrarily set to one. These currents specify the expansion coefficients $I_i^{(n)}$ for each element, which many then be used in (17) to obtain the current density on the resonator. If desired, the resulting modal current distribution can be renormalized in some convenient fashion.

C. Computation of Far-Field Natural Modes

Using (17)–(18) in (14), we find the contribution of the nth element to the far field pattern functions as

$$\mathcal{E}_{\theta,\varphi}^{(n)}(\hat{\boldsymbol{r}}) = \frac{k_0^2}{2\pi} e^{jk_0 d\cos\theta} \sum_{i=1}^{3} I_i^{(n)} \Bigg\{ \boldsymbol{G}_{\theta,\varphi}(\hat{\boldsymbol{r}}|z') \cdot \boldsymbol{l}_k^{(n)} \cdot \int_0^1 \int_0^{1-L_j'} e^{jk_0\hat{\boldsymbol{r}}\cdot\boldsymbol{\rho}'} L_j'\, dL_k'\, dL_j' - \boldsymbol{G}_{\theta,\varphi}(\hat{\boldsymbol{r}}|z') \cdot \boldsymbol{l}_j^{(n)} \int_0^1 \int_0^{1-L_j'} e^{jk_0\hat{\boldsymbol{r}}\cdot\boldsymbol{\rho}'} L_k'\, dL_k'\, dL_j' \Bigg\} \quad (25)$$

where $\boldsymbol{G}_{\theta}$ and $\boldsymbol{G}_{\varphi}$ are given by (15). The integrals in the above, which represent Fourier transforms of the area coordinates over triangular domains, can be done in closed form [39], or they may be approximated using a low-order numerical quadrature. Summing the individual contribu-

tions (25) over all triangular elements, we obtain the total pattern function of the resonator.

D. Evaluation of Spectral Integrals

The integration path of the Sommerfeld-type integrals (6), which appear in (8)–(10), must be properly indented around the singularities of the integrands [40], [3], [4]. These singularities include poles, which are the zeros in the k_ρ plane of the denominator function $\overleftrightarrow{Y}^p$ given in (29), and—for an open structure—a pair of branch points at $k_\rho = \pm k_0$, associated with the square root function $\kappa = \sqrt{k_0^2 - k_\rho^2}$ corresponding to the upper half-space, which we assume to have free space parameters. We note from (12) that k_0 is located in the first quadrant of the complex plane, and thus the branch points are in the first and third quadrants. It is convenient to introduce a two-sheeted k_ρ Riemann surface associated with κ, where the "proper" sheet is defined by the requirement that $\Im m\kappa < 0$, and the opposite holds on the other, "improper" sheet. These sheets are joined along a pair of branch cuts, which are specified by

$$k_\rho'^2 - k_\rho''^2 < k_0'^2, \quad k_\rho' k_\rho'' = \frac{k_0'^2}{2Q} \tag{26}$$

where we have introduced the notation $k_\rho = k_\rho' + jk_\rho''$ and $k_0' = 2\pi f_r \sqrt{\mu_0 \epsilon_0}$. These conditions define a pair of hyperbolae emanating from $\pm k_0$ in the first and third quadrants of the complex k_ρ plane. One of these branch cuts and two representative poles are shown in Fig. 4, which depicts the first quadrant of the proper k_ρ sheet. For an open structure, only a finite number of poles appear on the proper sheet. In Fig. 4, we also plot the integration path, which begins at the origin on the improper sheet, crosses the first-quadrant branch cut to emerge on the proper sheet, goes around the branch point and the poles, and proceeds to infinity along the real axis. Owing to the fact that a part of this path (denoted by a dashed line in Fig. 4) is on the improper sheet, the integrals in (8)–(10) become unbounded as $z \to \infty$, which is consistent with the remarks following (15). For finite z, these integrals are convergent, since the integration path approaches infinity on the proper k_ρ sheet. It should be noted that the path shown in Fig. 4 is equivalent to those used by other authors [40], [3], [4], even though they employ branch cuts different from those defined by (26) above.

The spectral integrals in (8)–(10) are evaluated on the path shown in Fig. 4 by a composite rule based on a low-order Gaussian quadrature, with various enhancements to improve efficiency, such as the method of averages [9]. To speed up the convergence of these integrals, we also subtract from the integrands their large-k_ρ forms. The latter can be integrated in closed form and they explicitly exhibit the source-region singularities of the corresponding integrals. Since a large number of Sommerfeld integrals must be computed to fill the impedance matrix at each frequency, we also employ a table look-up scheme

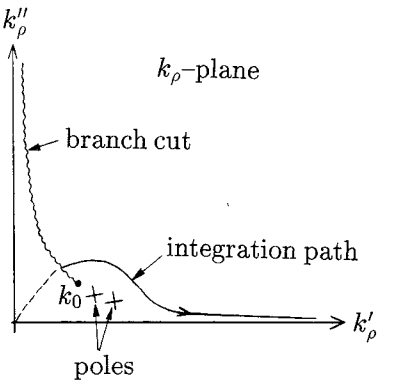

Fig 4. Integration path in the complex k_ρ-plane.

in conjunction with an interpolation method [41], [9] to reduce the solution time. We refer the reader to the literature for more details.

IV. Sample Results

In this section we present sample computed results, which serve to check the validity of the method, and also to demonstrate its flexibility and efficiency. Since data for comparison were not available for microstrip resonators having irregular shapes, most of the results included here are for circular and rectangular resonators.

The results in Figs. 5 through 7 are for a circular patch resonator, which was modeled by 184 triangular elements, as illustrated in Fig. 6. Observe that a nonuniform triangular mesh was used to better represent the singular behavior of the current near the edges of the patch. In Fig. 5 we compare the computed resonant frequency and the Q-factor of the circular disk patch, plotted versus the disk radius, with the corresponding measured and computed data obtained by Itoh and Mittra [42] and by Araki and Itoh [2], respectively. In Fig. 6(a) and (b) we superpose on the triangular mesh the vector plots of, respectively, the real and imaginary parts of the computed current distribution on a circular patch resonator of radius $a = 8$ mm, on an isotropic substrate of thickness $h = 1.5875$ mm and $\epsilon_r = 2.65$, at the dominant mode resonant frequency $f_r = 6.18626$ GHz. In Fig. 7 we compare the computed dominant far-field natural mode for a circular patch resonator on an isotropic substrate with $\epsilon_r = 2.65$ and $h/a = 0.0236$, with the corresponding data obtained by Araki and Itoh [2].

In Fig. 8 we show the computed normalized resonant length L/λ_0 of a rectangular patch resonator of width $W = 0.23\lambda_0$, where λ_0 is the free-space wavelength, on a uniaxial substrate with $\epsilon_z = 10.2$, versus the substrate thickness, for various values of ϵ_z. This configuration was previously analyzed by Pozar [43] using a spectral domain approach, and his data are also shown in Fig. 8. The rectangular patch was modeled by 140 triangular elements. In this case, while searching for the zeros of the matrix determinant, we used L and the imaginary part of f as the free parameters in the Müller method.

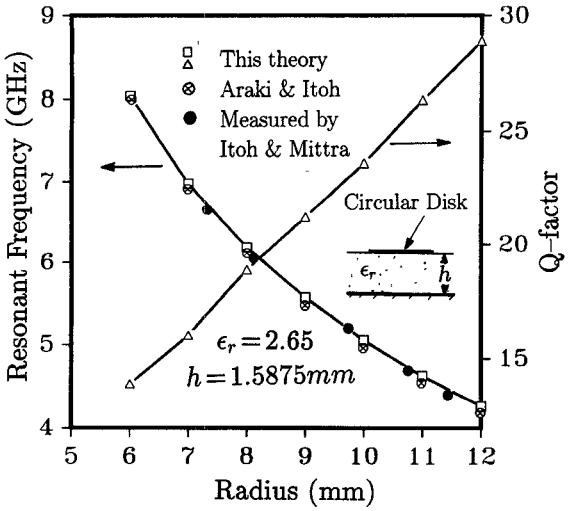

Fig. 5. Resonant frequency and Q-factor versus the radius a of a circular patch resonator on a substrate with $h = 1.5875$ mm and $\epsilon_r = 2.65$.

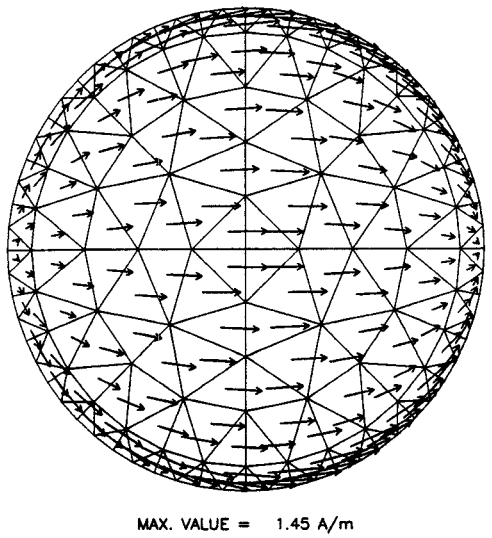

(a)

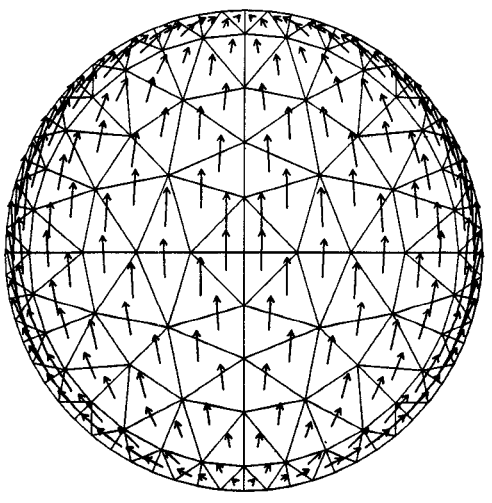

(b)

Fig. 6. Vector plot of the dominant mode current density on a circular patch resonator of radius $a = 8$ mm on a substrate with $h = 1.5875$ mm and $\epsilon_r = 2.65$, (a) Real part of the current. (b) Imaginary part of the current.

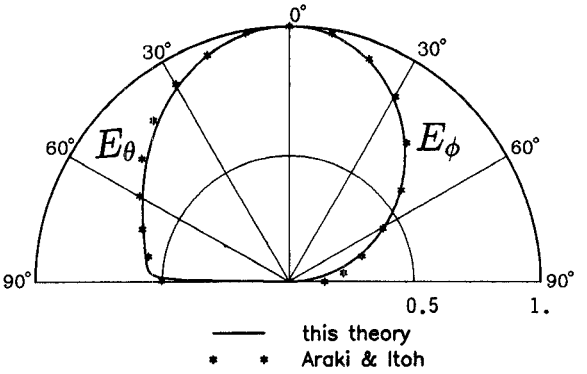

Fig. 7. Dominant far-field natural mode of a circular patch resonator on a substrate with $\epsilon_r = 2.65$ and $h/a = 0.0236$.

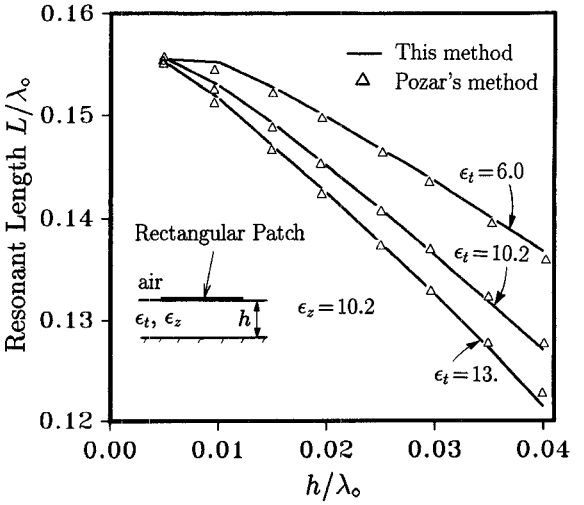

Fig. 8. Normalized resonant length of a rectangular patch resonator of width 0.23 λ_0 on a uniaxial substrate with $\epsilon_z = 10.2$, versus the substrate thickness, for various values of ϵ_t.

Finally, in Fig. 9 we plot the computed resonant frequency of an equilateral triangle patch resonator with a side length of 4 cm, on a uniaxial substrate with an isotropic cover layer, versus the substrate thickness, which is taken to be equal to that of the cover, for various values of the dielectric constants. These results illustrate the effect of the substrate anisotropy and the influence of the cover layer. No data for comparison were available in this case. The resonator was modeled by 144 nonuniform triangular elements, with smaller elements placed near the edges of the patch.

The formulation presented here has been implemented in FORTRAN on a PC with an $i486$ processor running at 25 MHz. The amount of computer time required to solve a typical case is modest, considering the generality and flexibility of the approach. For example, for the triangular patch resonator, for which results are given in Fig. 9, the computer time was approximately two minutes per iteration of the Müller method. With a reasonably good first guess, less than ten iterations were usually required to converge to a resonant frequency (or length).

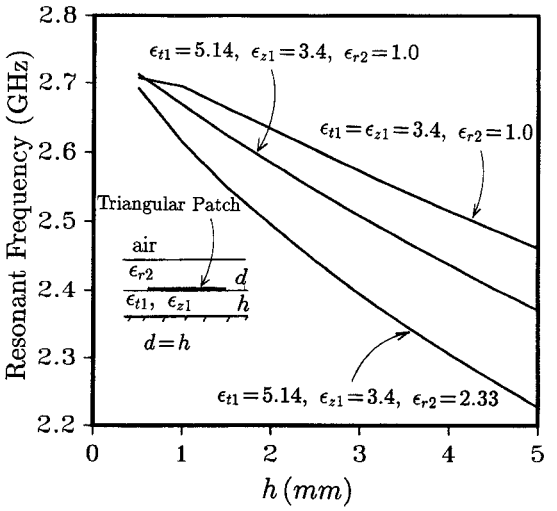

Fig. 9. Resonant frequency of an equilateral triangle patch resonator with a side length of 4 cm, on a uniaxial substrate with an isotropic cover layer, versus the substrate thickness, which is taken to be equal to that of the cover, for various values of the dielectric constants.

V. Conclusion

We have presented a method based on a space-domain MPIE formulation for the study of microstrip-patch resonators that are planar, but have otherwise arbitrary shape. The substrate may be uniaxially anisotropic and may consist of any number of homogeneous layers. The proposed approach, which incorporates a triangular element model of the patch and rigorously takes into account the radiation and guided wave losses, offers the flexibility and accuracy that make it ideal for the studies of irregularly shaped, single and multiple microstrip-patch resonators. However, it may not be the most efficient technique to use for everyday analyses of regular microstrip geometries for which simpler, specialized procedures may be available. An important application of this method will be as an aid in the development and validation of simple, approximate resonator models, required by computer-aided design packages.

Appendix
Transmission-Line Green's Functions

The propagation constant κ_n^p and the characteristic admittance Y_n^p of the nth section of the equivalent transmission-line network shown in Fig. 2 are given as

$$\kappa_n^e = \sqrt{k_0^2\epsilon_{tn} - k_\rho^2/\nu_n}, \quad \kappa_n^h = \sqrt{k_0^2\epsilon_{tn} - k_\rho^2} \tag{27}$$

$$Y_n^e = \frac{\omega\epsilon_0\epsilon_{tn}}{\kappa_n^e}, \quad Y_n^h = \frac{\kappa_n^h}{\omega\mu_0}. \tag{28}$$

We now introduce the transmission-line Green's functions $V_i^p(z|z')$ and $I_i^p(z|z')$ as, respectively, the voltage and the current at a point z, due to a unit-strength current source i, located at a point z' on the corresponding transmission-line network [25]. The dependence of these Green's functions on k_ρ is understood, and will be left out for brevity. Assuming, for simplicity, that the resonator is confined to the first two layers of the three-layer medium of Fig. 1 (i.e., $-h < z, z' < d$), we easily find the pertinent voltage transmission-line Green's function as [18, p. 29]

$$V_i^p(z|z') = \frac{\overleftarrow{V}_\alpha^p(z_<)\vec{V}_\alpha^p(z_>)}{\overleftrightarrow{Y}^p}, \quad \overleftrightarrow{Y}^p = \overleftarrow{Y}_1^p + \vec{Y}_2^p \tag{29}$$

where $z_<$ and $z_>$ denote, respectively, the lesser and the greater of z and z', and where the subscript α stands for 1 or 2 if the corresponding variable z or z' lies within the first or the second layer, respectively. The other symbols in (29) are defined as

$$\overleftarrow{V}_\alpha^p(z) = \cos\kappa_\alpha^p z + j\frac{\overleftarrow{Y}_1^p}{Y_\alpha^p}\sin\kappa_\alpha^p z,$$

$$\overleftarrow{Y}_1^p = -jY_1^p\cot\kappa_1^p h \tag{30}$$

$$\vec{V}_\alpha^p(z) = \cos\kappa_\alpha^p z + j\frac{\vec{Y}_2^p}{Y_\alpha^p}\sin\kappa_\alpha^p z,$$

$$\vec{Y}_2^p = Y_2^p\frac{Y_2^p - jY_3^p\cot\kappa_2^p d}{Y_3^p - jY_2^p\cot\kappa_2^p d} \tag{31}$$

where $\overleftarrow{Y}_1^p$ and $\vec{Y}_2^p$ are the leftward- and rightward-looking admittances at $z = 0$ on the first and second transmission line section, respectively. Once $V_i^p(z|z')$ has been found, the current Green's function $I_i^p(z|z')$ immediately follows from the transmission-line equation:

$$I_i^p(z|z') = -\frac{Y_n^p}{j\kappa_n^p}\frac{d}{dz}V_i^p(z|z'). \tag{32}$$

When the superstrate is absent, we simply set in the above $Y_3^p = Y_2^p$. In the case of a shielded resonator, having a conducting plate at $z = d$, we put $Y_3^p = \infty$. The generalization to an arbitrary number of dielectric layers in immediate.

References

[1] W. C. Chew and J A. Kong, "Resonance of nonaxial symmetric modes in circular microstrip disk antenna," *J. Math. Phys.*, vol. 21, pp. 2590-2598, Oct. 1980

[2] K. Araki and T. Itoh, "Hankel transform domain analysis of open circular microstrip radiating structures," *IEEE Trans. Antennas Propagat.*, vol. AP-29, pp. 84-89, Jan. 1981.

[3] S. Assailly, C. Terret, J. P. Daniel, G. Besnier, Mosig, and B. Roudot, "Spectral domain approach applied to open resonators: Application to microstrip antennas," *Electron. Lett.*, vol. 24, pp. 105-106, Jan. 1988.

[4] S. Nam and T. Itoh, "Calculation of accurate complex resonant frequency of an open microstrip resonator using the spectral domain method," *J. Electromagn. Waves Appl.*, vol. 2, no. 7, pp. 635-651, 1988.

[5] W. C. Chew, and Q. Liu, "Resonance frequency of a rectangular microstrip patch," *IEEE Trans. Antennas Propagat.*, vol. 36, pp. 1045-1056, Aug. 1988.

[6] K. M. Michalski and D. Zheng, "Analysis of planar microstrip structure of arbitrary shape—To be, or not to be in the spectral domain?," in *Proc. Symp. on Antenna Technology and Applied Electromagnetics*, ANTEM'90, University of Manitoba, Canada, Aug. 1990, pp. 240-245.

[7] J. R. Mosig, R. C. Hall, and F. E. Gardiol, "Numerical analysis of microstrip patch antennas," in *The Handbook of Microstrip Antennas*, J. R. James and P. S. Hall, Eds., Stevenage, UK: Peregrinus, 1989, pp. 393-453.

[8] J. R. Mosig, "Integral equation technique," in *Numerical Techniques for Microwave and Millimeter-Wave Passive Structures*, T. Itoh, Ed., pp. 133–213, New York: Wiley, 1989.
[9] J. R. Mosig and F. E. Gardiol, "A dynamical radiation model for microstrip structures," in *Adv. Electron Phys.*, P. W. Hawkes, Ed., New York: Academic 1982, vol. 59, pp. 139–237.
[10] A. W. Glisson and D. R. Wilton, "Simple and efficient numerical methods for problems of electromagnetic radiation and scattering from surfaces," *IEEE Trans. Antennas Propagat.*, vol. AP-28, pp. 593–603, Sept. 1980.
[11] J. R. Mosig, "Arbitrarily shaped microstrip structures and their analysis with a mixed potential integral equation," *IEEE Trans. Microwave Theory Tech.*, vol. 36, pp. 314–323, Feb. 1988.
[12] G. Kossiavas, A. Papiernik, J. P. Boisset, and M. Sauvan, "The C-Patch: A small microstrip element," *Electron. Lett.*, vol. 25, pp. 253–254, Feb. 1989.
[13] M. F. Cátedra and E. Gago, "Spectral domain analysis of conducting patches of arbitrary geometry in multilayer media using the CG-FFT method," *IEEE Trans. Antennas Propagat.*, vol. 38, pp. 1530–1536, Oct. 1990.
[14] P. Pichon, J. Mosig, and A. Papiernik, "Input impedance of arbitrarily shaped microstrip antennas," *Electron. Lett.*, vol. 24, pp. 1214–1215, Sept. 1988.
[15] M. J. Notter and C. G. Parini, "Modelling of arbitrary shaped M/S patch antennas in multiple substrate media," *Electron Lett.*, vol. 26, pp. 50–52, 1990.
[16] D. Zheng, and K. A. Michalski, "Analysis of arbitrarily shaped coax-fed microstrip antennas with thick substrates," *Electron. Lett.*, vol. 26, no. 12, pp. 794–795, 1990.
[17] S. M. Rao, D. R. Wilton, and A. W. Glisson, "Electromagnetic scattering by surfaces of arbitrary shape," *IEEE Trans. Antennas Propagat.*, vol. AP-30, pp. 409–418, May 1982.
[18] L. B. Felsen and N. Marcuvitz, *Radiation and Scattering of Waves*. Englewood Cliffs, NJ: Prentice-Hall, 1973.
[19] R. F. Harrington, *Time-Harmonic Electromagnetic Fields*. New York: McGraw-Hill, 1961.
[20] K. A. Michalski, "On the scalar potential of a point charge associated with a time-harmonic dipole in a layered medium," *IEEE Trans. Antennas Propagat.*, vol. AP-35, pp. 1299–1301, Nov. 1987.
[21] K. A. Michalski and D. Zheng, "Formulation of mixed-potential integral equations for arbitrarily shaped microstrip structures," *IEEE Trans. Microwave Theory Tech.*, to be published.
[22] P. Perlmutter, S. Shtrikman, and D. Treves, "Electric surface current model for the analysis of microstrip antennas with application to rectangular elements," *IEEE Trans. Antennas Propagat.*, vol. AP-33, pp. 301–311, Mar. 1985.
[23] N. K. Das and D. M. Pozar, "A generalized spectral-domain Green's function for multilayer dielectric substrates with application to multilayer transmission lines," *IEEE Trans. Microwave Theory Tech.*, vol. MTT-35, pp. 326–335, Mar. 1987.
[24] L. Vegni, R. Cicchetti, and P. Capece, "Spectral dyadic Green's function formulation for planar integrated structures," *IEEE Trans. Antennas Propagat.*, vol. 36, pp. 1057–1065, Aug. 1988.
[25] R. Kastner, E. Heyman, and A. Sabban, "Spectral domain iterative analysis of single- and double-layered microstrip antennas using conjugate gradient algorithm," *IEEE Trans. Antennas Propagat.*, vol. 36, pp. 1204–1212, Sept. 1988.
[26] Y. T. Lo, S. M. Wright, and M. Davidovitz, "Microstrip antennas," in *Handbook of Microwave and Optical Components*, K. Chang, Ed., New York: Wiley, 1989, vol. 1, pp. 764–888.
[27] W. C. Chew, "A quick way to approximate a Sommerfeld-Weyl-type integral," *IEEE Trans. Antennas Propagat.*, vol. 36, pp. 1654–1657, Nov. 1988.
[28] C. E. Baum, "The singularity expansion method," in *Transient Electromagnetic Fields*, L. B. Felsen, Ed., New York: Springer-Verlag, 1976, pp. 129–179.
[29] T. M. Willis and D. L. Sengupta, "Spectral analysis of microstrip antennas with CG-FFT: Two-dimensional results," *IEEE Trans. Antennas Propagat.*, vol. 37, pp. 810–816, July 1989.
[30] R. F. Harrington, *Field Computation by Moment Methods*. New York: Macmillan, 1968.
[31] L. Lapidus and G. F. Pinder, *Numerical Solution of Partial Differential Equations in Science and Engineering*. New York: Wiley, 1982.
[32] D. R. Tanner and A. F. Peterson, "Vector expansion functions for the numerical solution of Maxwell's equations," *Microwave & Opt. Tech. Lett.*, vol. 2, pp. 331–334, Sept. 1989.
[33] W. C. Chew, *Waves and Fields in Inhomogeneous Media*. New York: Van Nostrand Reinhold, 1990.
[34] S. U. Hwu and D. R. Wilton, "Electromagnetic scattering and radiation by arbitrary configurations of conducting bodies and wires," Tech. Rep. Applied Electromagnetics Lab., Dept. Elec. Eng., Univ. of Houston, Houston, TX, May 1988.
[35] K. A. Michalski and D. Zheng, "Integral Equation Analysis of Arbitrarily Shaped Microstrip Structures," Tech. Rep. Electromagnetics and Microwave Lab., Dept. Elec. Eng., Texas A&M Univ., June 1990.
[36] J. Van Bladel, *Electromagnetic Fields*. New York: Hemisphere, 1985.
[37] D. R. Wilton, S. M. Rao, A. W. Glisson, D. H. Schaubert, O. M. Al-Bundak, and C. M. Butler, "Potential integrals for uniform and linear source distributions on polygonal and polyhedral domains," *IEEE Trans. Antennas Propagat.*, vol. AP-32, pp. 276–281, Mar. 1984.
[38] S. D. Conte and C. de Boor, *Elementary Numerical Analysis: An Algorithmic Approach*. New York: McGraw-Hill, 1980.
[39] B. Houshmand, W. C. Chew, and S. W. Lee, "Fourier transform of a linear distribution with triangular support and its applications in Electromagnetics," *IEEE Trans. Antennas Propagat.*, vol. 39, pp. 252–254, Feb. 1991.
[40] W. C. Chew and J. A. Kong, "Resonance of the axial-symmetric modes in microstrip disk resonators," *J. Math. Phys.*, vol. 21, pp. 583–591, Mar. 1980.
[41] G. J. Burke, E. K. Miller, J. N. Brittingham, D. L. Lager, R. J. Lytle, and J. T. Okada, "Computer modeling of antennas near the ground," *Electromagn.*, vol. 1, no. 1, pp. 29–49, 1981.
[42] T. Itoh and R. Mittra, "Analysis of a microstrip disk resonator," *Arch. Elek. Übertragung.*, vol. 27, no. 11, pp. 456–458, 1973.
[43] D. M. Pozar, "Radiation and scattering from a microstrip patch on a uniaxial substrate," *IEEE Trnas. Antennas Propagat.*, vol. AP-35, pp. 613–621, June 1987.

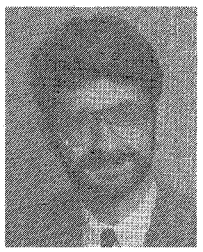

Krzysztof A. Michalski (S'78–M'81–SM'88) was born in Poland. He received the M.S. degree from the Technical University of Wroclaw, Wroclaw, Poland, in 1974 and the Ph.D. degree from the University of Kentucky in 1981, both in electrical engineering.

From 1982 to 1986, he was Assistant Professor at the University of Mississippi. In 1987, he joined Texas A&M University, College Station, TX, where he is presently Associate Professor of Electrical Engineering. His current research interests include analytical and numerical methods for the solution of boundary value problems of electromagnetics.

Dr. Michalski is a member of the Institution of Electrical Engineers (IEE) and of Commission B (Fields and Waves) of the International Union of Radio Science (URSI). He was a U.S. delegate to the URSI General Assembly in 1984. Also in 1984, he received the Best EMP Paper Award from the Summa Foundation, and in 1986, he was awarded the Oliver Lodge Premium by the IEE.

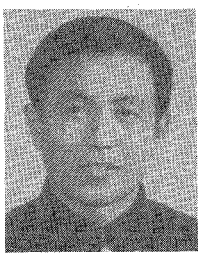

Dalian Zheng (S'85–M'89) was born in Liaoning, People's Republic of China, in 1955. He received the B.E. degree from the Beijing Institute of Aeronautics and Astronautics in 1982, the M.Sc. degree from the Ohio State University in 1985, and the Ph.D. degree from the University of Mississippi in 1988, all in electrical engineering.

From 1985 to 1987, he was Graduate Research Assistant at the University of Mississippi, and from 1987 to 1988 at Texas A&M University, College Station, TX, where he is presently a Research Associate in the Department of Electrical Engineering. His major research interests are electromagnetic theory, numerical methods applied to scatters and antennas of arbitrary shape in complex environments, and microstrip transmission lines.